JOURNAL OF SOLID STATE CHEMISTRY 69, 230–239 (1987)

Structural and Dynamical Studies of δ-Bi_2O_3 Oxide Ion Conductors

IV. An EXAFS Investigation of $(Bi_2O_3)_{1-x}(M_2O_3)_x$ for M = Y, Er, and Yb

P. D. BATTLE,* C. R. A. CATLOW,† A. V. CHADWICK‡, P. COX,† G. N. GREAVES,§ AND L. M. MORONEY‖,[1]

Department of Inorganic and Structural Chemistry, Leeds University, Leeds LS2 9JT, †Department of Chemistry, University of Keele, Keele, Staffordshire ST5 5AG, ‡Department of Chemistry, University of Canterbury, Canterbury, Kent CT2 7NH, §SERC, Daresbury Laboratory, Daresbury, Warrington WA4 4AD, United Kingdom, and ‖NSLS, Brookhaven National Laboratory, Upton, New York 11973

Received September 2, 1986

The local structural environments of Bi^{3+} and dopant cations in the fluorite-structured solid solutions $(M_2O_3)_x(Bi_2O_3)_{1-x}$ (M = Y, Er, Yb) have been studied using extended X-ray absorption fine structure techniques. The results show that the Bi–O shell is heavily disordered with an asymmetric radial distribution function. The Bi^{3+} ion tends to be displaced from its centrosymmetric, cube center site. The first coordination shell of the dopant is comparatively ordered. Varying the dopant cation has a small effect on the local structural environment and increasing the dopant concentration causes a small increase in the degree of local order. Data obtained over a range of temperatures show that the large anisotropy in the Bi–O shell is attributable to static displacements from the perfect lattice sites. The degree of correlation between the thermal vibrations of the anion sublattice and those of the Bi atoms differs from that observed between those of the anion sublattice and the dopant atoms; the significance of this for ionic conductivity is discussed.

Introduction

Bi_2O_3 undergoes a phase transition from a monoclinic structure to the fluorite-structured δ phase at 1003 K which is accompanied by a jump in oxide ion conductivity of more than three orders of magnitude (*1*). It has been shown that the addition of certain trivalent cations, such as Y^{3+}, and the smaller rare earths, for example, Er^{3+} or Yb^{3+}, stabilizes the δ phase down to room temperature, yielding compounds with ionic conductivities of the order of $10^{-2}\ \Omega^{-1}\ cm^{-1}$ at 770 K (*2*, *3*) compared with $10^{-3}\ \Omega^{-1}\ cm^{-1}$ for both the pure material and yttria-stabilized zirconia, the benchmark for anion conductors to date (*4*).

The dopant concentration range over which the fluorite phase is formed varies with the trivalent cation used and has yet to be unequivocally determined for all dopants. However, it appears to be generally true that the smaller the dopant cation ra-

[1] Author to whom correspondence should be addressed.

0022-4596/87 $3.00

dius, the lower the concentration needed to form the fluorite phase (*2*). Also, the highest ionic conductivities are observed for the phases with the lowest dopant concentration. Thus, for Y_2O_3 and those rare earths that form the fluorite phase, $(M_2O_3)_x(Bi_2O_3)_{1-x}$, the lower limit for x decreases from 0.4 for Sm^{3+} to 0.2 for Er^{3+} and Y^{3+}. The best conductor is $(Er_2O_3)_{0.2}(Bi_2O_3)_{0.8}$ with $\sigma = 2.3 \times 10^{-2}\ \Omega^{-1}\ cm^{-1}$ at 770 K (*2, 3*).

That Bi_2O_3 and M_2O_3/Bi_2O_3 solid solutions adopt the fluorite structure at all is remarkable in that the M_2O_3 stoichiometry requires the MO_2-fluorite structure formed to have two anion vacancies per unit cell. Our neutron scattering studies of these materials reveal that in addition to these vacancies, there is substantial anion disorder in the structure with ~30% of the anions being displaced 0.66 Å in ⟨111⟩ directions, and a further 5% occupying the 48*i* sites at ($\frac{1}{2}$, 0.3, 0.3), roughly midway between two lattice anion sites. The cations exhibit small ⟨100⟩ displacements (*5, 11*).

The lower the M_2O_3 dopant concentration in the solid solutions, the greater is the number of ⟨111⟩ displaced anions observed. Diffuse elastic neutron scattering evidence also showed that there is an increase in short-range ordering (probably on the anion sublattice) as the dopant cation concentration increases. We interpreted these results in terms of a dopant cation–induced ordering of the anion vacancies in strings along the ⟨111⟩ and ⟨110⟩ directions of the unit cell. Our model postulated that Bi^{3+}, with its stereochemically active lone pair of electrons, may prefer a noncentrosymmetric anion distribution with the pair of oxygen ion vacancies disposed along a face-diagonal ⟨110⟩ direction of the anion sublattice. We envisaged that the lone electron pair on Bi^{3+} may be directed toward this oxygen-deficient face, perhaps accounting for the observed ⟨100⟩ cation displacements, with relaxations in the ⟨111⟩ direction of some of the remaining oxide ions to envelop the Bi^{3+} ion.

Thus, this model implies that a different local structural environment is preferred by Bi^{3+} compared with the dopant ion, in spite of their occupying crystallographically indistinguishable sites in the average unit cell. To test this hypothesis, we have used the technique of extended X-ray absorption fine structure (EXAFS) spectroscopy to compare the local structural environments of the two different cations and to attempt to determine how this environment is affected by different dopants, different dopant concentrations, and temperature.

The EXAFS Technique

The EXAFS experiment measures the oscillations observed on the high-energy side of an X-ray absorption edge. These arise because of interference between the outgoing photoelectron wave and that fraction of itself which is backscattered by neighboring atoms, and thus the fine structure contains information on the number, type, and distance of the neighbors surrounding atoms of the absorbing species. Thus, by collecting the EXAFS on the $Bi(L_{III})$ and $Er(L_{III})$ edges, for example, we are able to probe directly and easily the distribution of oxygen ions about the two cations and to determine if their environments are indeed different.

The EXAFS spectra of Bi and Er in $(Er_2O_3)_{0.4}(Bi_2O_3)_{0.6}$ are plotted in Fig. 1. The oscillations have been separated from the smoothly decreasing X-ray absorbance past the edge in the normal way and the normalized oscillatory data (χ) have been plotted versus the momentum (k) of the photoelectron ejected in the absorption process. χ is weighted by k^3 to show the data at high k more clearly.

The k-dependence of χ can be described by the so-called plane wave equation (for a

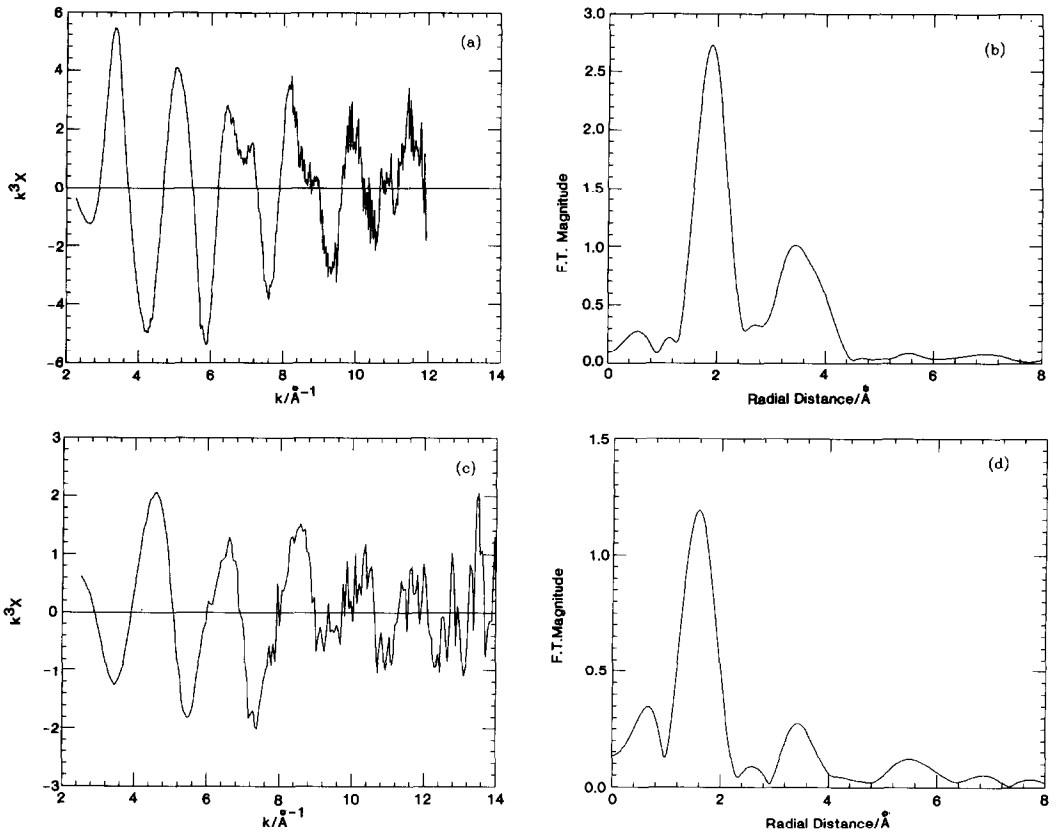

FIG. 1. (a) k^3-weighted EXAFS from the Er L_{III} edge of 40% Er_2O_3/Bi_2O_3 at 80 K. (b) The magnitude of the Fourier transform of the data in (a). (c) k^3-weighted EXAFS from the Bi L_{III} edge of 40% Er_2O_3/Bi_2O_3 at 80 K. (d) The magnitude of the Fourier transform of the data in (c).

comprehensive description of the technique, see Refs. (*6–8*)):

$$\chi(k) = \sum_j \frac{N_j}{kR_j^2} |f_j(\pi, k)| \exp(-2\sigma_j^2 k^2) \sin(2kR_j + 2\delta_1 + \psi_j). \quad (1)$$

The frequency of the oscillations depends on R_j, the distance between the excited atom (Bi or Er) and its jth shell of neighbors (e.g., six oxygens for $j = 1$). The two additional terms, δ_1 and ψ_j, are the shifts in phase experienced by the photoelectron wave in passing through the atomic potential of the central atom and the jth shell of backscattering atoms, respectively. The amplitude of χ depends on N_j, the number of atoms in shell j, and its inverse dependence on R_j^2 results in the nearest neighbors, generally, contributing most to the overall EXAFS. Consequently, structural data are most easily determined for the nearest neighbors. The Debye–Waller factor ($\exp(-2\sigma_j^2 k^2)$) allows for amplitude reduction arising from a Gaussian spread of component distances within the jth shell due to static displacements and thermal motion. σ_j^2 is the statistical variance in the value of R_j. $|f_j(\pi,k)|$ is a k-dependent function describing the backscattering power of the jth-shell neighbors. Thus, it is $f_j(\pi, k)$ and ψ_j which allow one, in principle, to distinguish

between different types of neighbors, in that O^{2-} backscatters photoelectrons more weakly than Bi^{3+} for most values of k.

The magnitude of the Fourier transform of $\chi(k)$ with respect to $2kr$ resembles a radial distribution function wherein peaks corresponding to the successive shells of neighbors appear at increasing distances from the central atom but shifted ~0.5 Å to low R owing to the phase terms δ_1 and ψ_j. However, unlike a true radial distribution function, the intensity of the peaks in the magnitude of the Fourier-transformed data depends on the same amplitude parameters as in Eq. (1), including σ_j, $|f_j(\pi, k)|$, and $1/R_j^2$. The latter factor means that high-r features in the data tend to be overshadowed by the low-r data and that asymmetric distributions which are typical of ionic conductors do not show up as well as in Fourier-transformed data as in true radial distribution functions.

In order to quantify the structural environments of the cations in our samples, it is necessary to calculate the functions $|f_j(\pi, k)|$, $\delta_1(k)$, and $\psi_j(k)$. This was done using the muffin tin approximation (*9, 10*) and the validity of the functions verified by using them to fit structural standards such as monoclinic Bi_2O_3, Er_2O_3, and Y_2O_3.

Experimental

The composition of the samples used in this study include $(Y_2O_3)_x(Bi_2O_3)_{1-x}$, x = 0.27, 0.34, 0.40; $(Er_2O_3)_x(Bi_2O_3)_{1-x}$, x = 0.2, 0.32, 0.4; and $(Yb_2O_3)_x(Bi_2O_3)_{1-x}$, x = 0.2, 0.25, 0.3, 0.35, and were prepared according to the method described previously (*5*). These samples were mixed with sufficient BN to yield a mixture with an X-ray absorbance $\ln(I_0/I)$ of ~1 past the absorption edges. EXAFS spectra were measured using stations 7.1 and 9.2 on the Synchrotron Radiation Source at Daresbury Laboratory. Data were collected at room temperature and 80 K for 300 eV below to 1000 eV above the Er L_{III} (8358 eV), Yb L_{III} (8943 eV), Bi L_{III} (13,418 eV), and Y K (17,080 eV) edges. In addition, $(Y_2O_3)_{0.4}(Bi_2O_3)_{0.6}$ and $(Er_2O_3)_{0.25}(Bi_2O_3)_{0.75}$ were heated and EXAFS data collected at temperatures between 80 and 1000 K.

Results

(*i*) *Comparing Dopant and Bi^{3+} Structural Environments*

Figure 1 shows a typical pair of EXAFS spectra and their Fourier transforms for the dopant and Bi L_{III} edges in the solid solution of composition, $(Er_2O_3)_{0.4}(Bi_2O_3)_{0.6}$. The EXAFS spectra resemble one another in that each consists of a dominant frequency representing backscattering from the six oxygen nearest neighbors. However, the amplitude of the Er L_{III} EXAFS is nearly three times that of the Bi EXAFS as can be seen in the k-space plots and the r-space Fourier-transformed data. Similarly, the second shell of cation neighbors at ~3.6 Å is clearly detectable for Er, but the amplitude of the Bi–cation feature is significantly lower. More distant shells are not visible in the Fourier-transformed data for either cation. This gives some indication of the level of disorder in these materials. The parent materials, Er_2O_3 and monoclinic Bi_2O_3, both exhibit peaks out to 5–6 Å from the central atom. In Er_2O_3/Bi_2O_3, therefore, there is clearly a large degree of deviation of the atoms from the perfect lattice sites such that the coherence of scattering from shells more remote than the second is reduced to the point where their EXAFS contributions are reduced to the noise level. Furthermore, from the fact that the amplitude of the Bi–O EXAFS is less than that of the Er–O EXAFS, we can infer that the degree of disorder within the Bi–O shell is greater than that in the Er–O shell. The amplitude terms N_1 and $|f_1(\pi)|$ are the same for both cations, leaving only the parame-

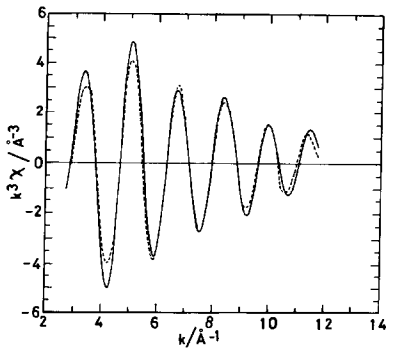

FIG. 2. The Fourier-filtered, k^3-weighted EXAFS data for the nearest-neighbor Er–O shell in 40% Er_2O_3/Bi_2O_3 (solid line) and theoretical fit obtained with six oxygen atoms at 2.27 Å and σ^2 of 0.013 Å^2 (dashed line).

ters R_1 and σ_1^2 to account for the amplitude difference (Eq. (1)).

In order to quantify this difference, we used Fourier filtering to isolate the first-shell EXAFS for each cation and fitted the data using the calculated phase shifts to determine R_1 and σ_1^2. Figure 2 shows that the Er–O EXAFS can be modelled reasonably well by six oxygen neighbors at a distance of 2.27 Å. In fact, comparison of these data with those for pure Er_2O_3 shows that the local structural environment of Er in $(Er_2O_3)_{0.4}(Bi_2O_3)_{0.6}$ more closely resembles that of Er in Er_2O_3 than it does the crystallographically equivalent Bi environment in the solid solution. There are two crystallographic sites occupied by Er in Er_2O_3, one in which the Er is coordinated to six oxygens at a distance of 2.28 Å and the other where there are two oxygen atoms at 2.20 Å, two at 2.21 Å, and two at 2.30 Å. Thus, the average Er–O distance is 2.27 Å but with a standard deviation of 0.04 Å. The similarity between the Er–O EXAFS in the solid solution and the parent oxide leads us to suspect that the local structural environment in the former also exhibits non-Gaussian static disorder within the shell, in which case using a Debye–Waller factor of the form in Eq. (1) is clearly inappropriate. The mismatch in phase between the calculated and measured EXAFS at high k gives some intimation of this.

Figure 3 shows the result of a least-squares fit of six oxygen atoms to the Bi–O EXAFS, where $R_1 \sim 2.11$ Å and $\sigma_1^2 \sim 0.050$ Å^2. The inadequacy of this fit indicates that, certainly for the Bi–O EXAFS, the assumption that disorder within the shell can be accommodated by a Gaussian distribution is not valid. Loss of phase matching between theory and experiment at high k is a typical manifestation of anisotropy in a shell of backscatterers (*8, 12*).

For this reason we fitted the data by constraining the total number of atoms to be equal to six but allowing the distance and Debye–Waller factor of all of the atoms in the shell to float to obtain a good fit to the experimental data over all k. Clearly, the individual values for R_j and σ_j for each of the component atoms are too highly correlated to yield any significant information, but it is possible to construct from these values a true atomic radial distribution function of oxygen atoms about Bi. The

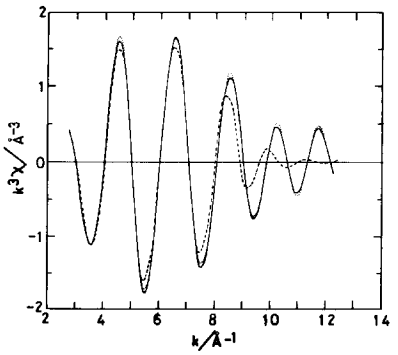

FIG. 3. The Fourier-filtered, k^3-weighted EXAFS Data for the nearest-neighbor Bi–O shell in 40% Er_2O_3/Bi_2O_3 (solid line) and theoretical fit obtained with six oxygen atoms at 2.11 Å and σ^2 of 0.025 Å^2 (dashed line). The dotted line represents the theoretical fit obtained in k space for the radial distribution plotted in Fig. 4a (see text for details).

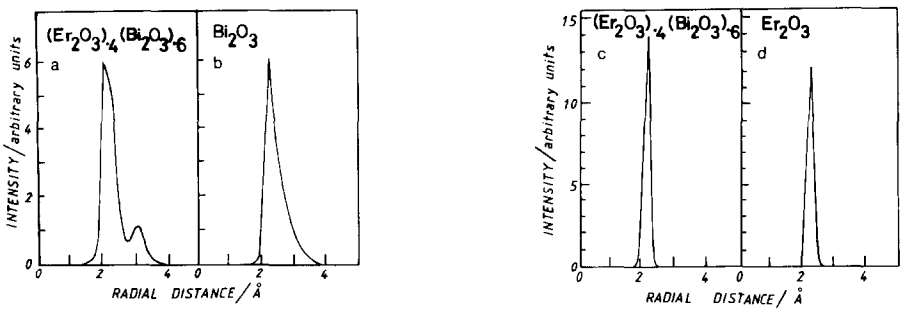

FIG. 4. Radial distribution functions of oxygen neighbors of Bi and Er constructed from the values of six cation–oxygen distances and one Debye–Waller factor floated in a least-squares fit to the Fourier-filtered EXAFS data for the first shell of oxygen neighbors for Bi and Er. (a) Bi–O RDF for 40% Er_2O_3/Bi_2O_3, (b) Bi–O RDF for monoclinic Bi_2O_3, (c) Er–O RDF for 40% Er_2O_3/Bi_2O_3, and (d) Er–O RDF for Er_2O_3.

RDFs determined in this way are plotted in Fig. 4 for the Bi–O EXAFS in Er_2O_3/Bi_2O_3 and Bi_2O_3 and the Er–O EXAFS in Er_2O_3/Bi_2O_3 and Er_2O_3. The comparatively large asymmetry for the Bi–O in the solid solution bears some resemblance to the RDF for pure Bi_2O_3, which has two crystallographic sites for Bi with a wide spread in Bi–O distances from 2.13 to 2.79 Å. The mean Bi–O distance is 2.37 Å with a standard deviation of 0.23 Å (*13*).

The small peak at 3.1 Å in the RDF of Bi–O in the solid solution is at a distance close to that expected for the displaced anions in the 48*i* sites seen in the neutron scattering experiments and it is interesting to speculate that these are associated preferentially with Bi in these materials.

The fact that the second-shell amplitude is less in the Bi EXAFS than in the Er data indicates that the disorder associated with Bi involves the Bi ions tending to be displaced from their centrosymmetric sites. Any displacement from the center of the 12 cation second neighbors would result in a spread of Bi–cation distances and consequently an increase in Debye–Waller factor and decrease in amplitude. This result would indicate that it is the Bi ions rather than the dopant that undergo the ⟨100⟩ cation displacements observed in the diffraction experiments (*5*).

(ii) *Effect of Different Dopant Cations*

There are no large changes in the EXAFS when the dopant cation is changed from Er to Y or Yb. Figure 5 shows the Fourier-transformed data for 40% M_2O_3/Bi_2O_3 (M = Y and Er) and 35% Yb_2O_3/Bi_2O_3, these being the highest dopant concentrations we found to form the fluorite phase. The ampli-

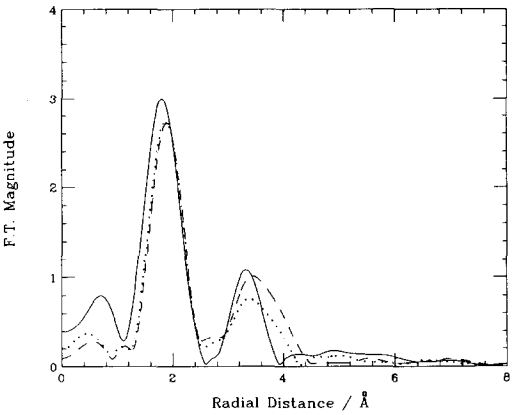

FIG. 5. A comparison of the Fourier-transformed dopant edge EXAFS for 4)% Y_2O_3/Bi_2O_3 (solid line), 40% Er_2O_3/Bi_2O_3 (dashed line), and 35% Yb_2O_3/Bi_2O_3 (dotted line) at 80 K.

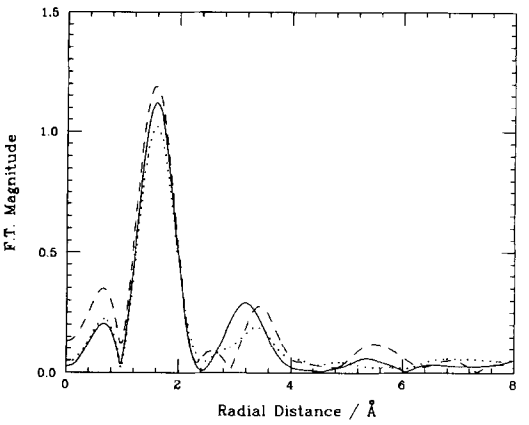

FIG. 6. A comparison of the Fourier-transformed EXAFS data for the Bi edges of 40% Y_2O_3/Bi_2O_3 (solid line), 40% Er_2O_3/Bi_2O_3 (dashed line), and 35% Yb_2O_3/Bi_2O_3 (dotted line) at 80 K.

tude in the first shell for Y–O is a little greater than for Er, suggesting that the Y may enhance the ordering of its oxygen shell somewhat more than Er, which could be attributed to their different polarizabilities. (The difference in the positions of the first-shell maxima is a result of the central atom phase shift, δ, being larger for Er and Yb than for Y.)

The second shell in the Fourier transform at ~3.6 Å is approximately the same amplitude for all three dopants. Since the amplitude depends on the backscattering function of the neighboring atoms, Y, Er, Yb, and Bi, and these functions show quite a large difference in their k dependencies (*14*), this results in differences in the general shape of the second shell in the Fourier transform. However, there are clearly no gross differences between the local environments of the different dopant cations.

The Bi edge data in Fig. 6 show that the amplitude of the first shell decreases slightly with the Y-doped sample having the most order and Yb the least. The second shells also decrease in amplitude in the same order although the structure in this shell for the different cations obscures this and makes it difficult to draw any firm conclusions.

(*iii*) *Effect of Dopant Concentration*

Increasing the dopant concentration across the composition range of the fluorite structure causes a small increase in amplitude of the EXAFS of both dopant and Bi edges, providing further evidence for the correlation between increasing dopant concentration and decreasing local static disorder within the materials.

(*iv*) *Effect of Temperature*

One way to ascertain if the anisotropy observed for the Bi EXAFS is due to thermal disorder or static displacements from the crystallographic sites is to obtain data at different temperatures. All of the concentrations were measured at liquid nitrogen temperatures and room temperature. If the large anisotropy observed in the local structural environment of the Bi^{3+} ions were attributable to large thermal vibrations, we would expect to see a significant change in the EXAFS with increase in temperature. Figure 7 shows a typical comparison of the

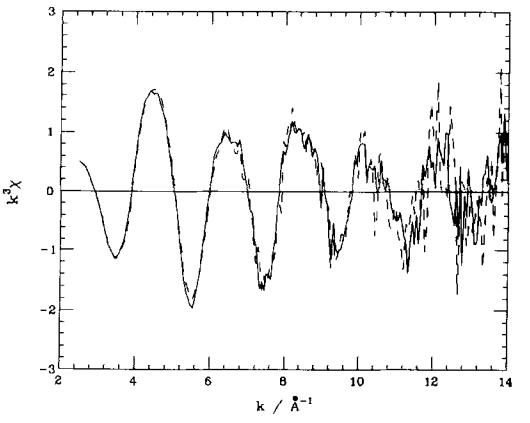

FIG. 7. A comparison of the k^3-weighted EXAFS on the Bi edge of 40% Y_2O_3/Bi_2O_3 at 80 K (solid line) and at room temperature (dashed line).

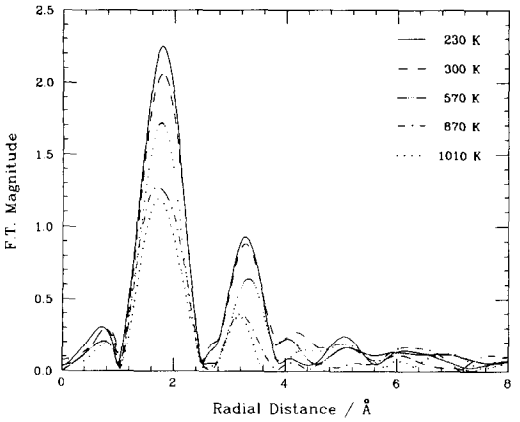

FIG. 8. The Fourier-transformed data for the Y edge EXAFS of 40% Y_2O_3/Bi_2O_3 over the temperature range 230 to 1020 K.

data in k space at the two temperatures for 40% Y_2O_3/Bi_2O_3 at the Bi edge. The minimal change in amplitude with temperature is confirmation that the observed anisotropy is indeed due to static displacements of the ions from their perfect lattice sites.

Two of the samples were heated over a wider temperature range. Figures 8 and 9 show the Fourier-transformed data of the Y edge and Bi edge data for 40% Y_2O_3/Bi_2O_3. The data obtained for the Er sample behaved similarly. All features decrease in amplitude as the temperature increases and the thermal component of the Debye–Waller factor increases. The Y–O amplitude decreases more than the Bi–O amplitude although its value at 1020 K is comparable to that of Bi–O at 80 K. Thus, the thermally induced increase in disorder in the Y–O shell at 1020 K matches that in the Bi–O shell attributed to static effects at 80 K. That the effect of temperature on the Y–O EXAFS is greater than that on the Bi–O EXAFS is evidence that the Bi–O interaction is more covalent in nature than the Y–O interaction.

The effect of temperature is expected to be larger for more distant shells since the greater the distance between central atom and backscatterer, the less highly correlated their thermal motions will be, and so the effect of temperature on the second shells is larger than for the nearer neighbors. However, comparing the Y–cation with the Bi–cation second-shell temperature dependence, it can be seen that the Bi–cation peak decreases in amplitude more rapidly than the Y–cation peak. Thus, although the Bi and oxygen ions are comparatively tightly bound, the whole (BiO_6) entity vibrates such that the spread in the Bi–cation second-neighbor distances increases more rapidly with temperature than is observed for the Y–cation distances.

Discussion

The foregoing EXAFS results show that, in spite of the dopant and Bi cations occupying crystallographically equivalent sites in the fluorite lattice, local structural disorder results in their immediate environments being quite different. We have seen that both cations have local structural configurations which resemble their parent oxides. Thus, Bi^{3+} has a highly disordered first shell of oxygen neighbors and tends, also, to be

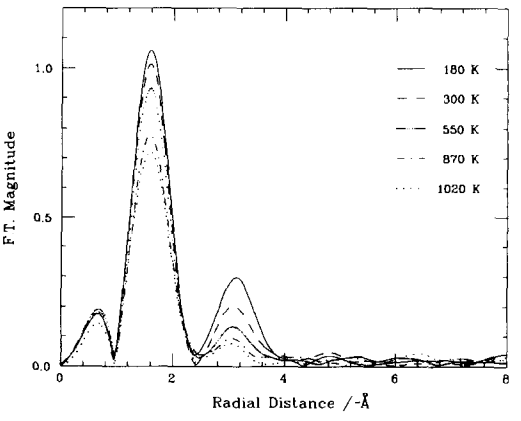

FIG. 9. The Fourier-transformed data for the Bi EXAFS of 40% Y_2O_3/Bi_2O_3 over the temperature range 180 to 1020 K.

displaced from its cube-center site. This behavior must arise from the highly polarizable nature of the cation with its lone electron pair. Disorder in the Bi–O shells must necessarily impose a certain measure of disorder on the dopant oxygen shells but the evidence here shows that the dopant ions achieve a significantly more ordered local environment. One can consider that the structural rôle of the dopant is to absorb the anion disorder generated about the Bi ions and thus rectify local deviations from the periodicity of the fluorite structure. This would account for the fact that only the small rare earth dopants stabilize the fluorite M_2O_3/Bi_2O_3 phase—the larger volume occupied by the rare earths of lower atomic number would preclude their being able to absorb as much anion disorder. Y^{3+}, Er^{3+}, and Yb^{3+} are all smaller than the volume available at the center of the anion "cubes" in the fluorite structure. In terms of this picture, it is easy to understand why increasing the dopant concentration increases the order within the structure.

The three different dopants studied appear to behave in the same way: the small differences between the spectra suggest that Y-doped samples are slightly more ordered than Er and both more so than Yb, but these differences are slight and this conclusion must be tentative.

The high-temperature experiments show that the dopant cation has the more typically ionic behavior, there being a larger increase in thermal motion in the Y–O interaction with temperature than in the Bi–O interaction. The Bi–O vibrations are more strongly correlated but since EXAFS data inherently weight nearer neighbors rather than more distant ones, we must distinguish between the very nearest oxygen neighbors and the more remote oxygen atoms. From the RDFs, we see that Bi^{3+}, putatively the larger cation, has a range of Bi–O distances varying from shorter than the dopant oxygen distance to significantly longer (Fig. 4). It may well be that the existence of very short, strongly bound oxygens reduces the need of the Bi always to be 6 coordinate. Thus, although the short Bi–O bond vibrations are highly correlated, the same is not necessarily true of those of the long Bi–O bonds, which may not be unduly difficult to break. Furthermore, the fact that the highest conductivities occur when the Bi : dopant ratio is maximized also indicates that the source of the conducting anions is the Bi–O shell. It would, therefore, seem reasonable to postulate that it is the distant oxygen atoms that take part in the anion conduction and loss of such remote oxygen ions would have an imperceptible effect on the measured EXAFS.

Although the Bi and anion vibrations are more strongly correlated than the dopant and anion vibrations, the Bi–cation vibrations are less strongly correlated than the dopant–cation vibrations. This would suggest that the dynamics of the oxygen sublattice tend to follow the Bi^{3+} thermal vibrations, whereas the dopant ions vibrate randomly about their centrosymmetric site.

To link the short-range structural information gathered here with our previous neutron scattering data, we note that the EXAFS data confirm our prediction that Bi^{3+} is less likely to adopt a centrosymmetric distribution of anions. Also, the EXAFS results show that it is reasonable to associate the observed ⟨100⟩ displacements with the Bi^{3+} ions. Seeing no structure in the EXAFS data from shells of neighbors more distant than the second, we are unable to draw any direct conclusions about the nature of the intermediate-range ordering we have observed in the diffuse elastic neutron scattering experiments. However, the model we proposed suggested that the dopant cations adopted an anion/vacancy distribution similar to that in the parent C-type rare earth materials, and, as noted, the immediate local structural environment of the dopants confirms this picture.

Acknowledgments

We thank the Science and Engineering Research Council and staff of Daresbury Laboratory for the provision of synchrotron radiation and related facilities. The financial support of the SERC (GR/D/02041) and the U.S. D.O.E. (DE-AS05-80-ER10742) is gratefully acknowledged. P.D.B. thanks the Research Corporation Trust for support.

References

1. T. Takahashi and H. Iwahara, *Mater. Res. Bull.* **13,** 1447 (1978).
2. H. Iwahara, T. Esaka, T. Sato, and T. Takahashi, *J. Solid State Chem.* **39,** 173 (1981).
3. M. J. Verkerk, K. Keizer, and A. J. Burgraaf, *J. Appl. Electrochem.* **10,** 81 (1980).
4. T. H. Etsell and S. N. Flengas, *Chem. Rev.* **70,** 339 (1970).
5. P. D. Battle, C. R. A. Catlow, J. W. Heap, and L. M. Moroney, *J. Solid State Chem.* **63,** 8 (1986).
6. E. A. Stern, *Contemp. Phys.* **19,** 289 (1978).
7. P. A. Lee, P. H. Citrin, P. Eisenberger, and B. M. Kincaid, *Rev. Modern Phys.* **53,** 769 (1981).
8. T. M. Hayes and J. B. Boyce, *Solid State Phys.* **37,** 173 (1984).
9. P. A. Lee and J. B. Pendry, *Phys. Rev. B* **11,** 2795 (1975).
10. J. B. Pendry, *in* "Low Energy Electron Diffraction," Academic Press, New York (1974).
11. P. D. Battle, C. R. A. Catlow, and L. M. Moroney, *J. Solid State Chem.* **67,** 42–50, (1987).
12. J. B. Boyce and T. M. Hayes, *in* "Physics of Superionic Conductors" (M. B. Salamon, Ed.), pp. 5–35, Springer-Verlag, Berlin (1979).
13. H. A. Harwig, *Z. Anorg. Allg. Chem.* **444,** 151 (1978).
14. B. K. Teo and P. A. Lee, *J. Amer. Chem. Soc.* **101,** 2815 (1979).